NeuroImage: Clinical 34 (2022) 103016

Contents lists available at ScienceDirect

NeuroImage: Clinical

journal homepage: www.elsevier.com/locate/ynicl

Early and progressive dysfunction revealed by *in vivo* neurite imaging in the rNLS8 TDP-43 mouse model of ALS

Akram Zamani [a], Adam K. Walker [b], Ben Rollo [a], Katie L. Ayers [c,d], Raysha Farah [a], Terence J. O'Brien [a,e], David K. Wright [a,*]

[a] Department of Neuroscience, Central Clinical School, Monash University, Melbourne, VIC 3004, Australia
[b] Queensland Brain Institute, The University of Queensland, QLD 4072, Australia
[c] The Murdoch Children's Research Institute, The Royal Children's Hospital, Parkville, VIC 3052, Australia
[d] Department of Pediatrics, The University of Melbourne, Parkville, VIC 3052, Australia
[e] Department of Medicine, The Royal Melbourne Hospital, The University of Melbourne, Parkville, VIC 3052, Australia

ARTICLE INFO

Keywords:
NODDI
DTI
Neurodegeneration
Motor neurone disease
MRI

ABSTRACT

Amyotrophic lateral sclerosis (ALS) is characterized by transactive response DNA-binding protein 43 (TDP-43) pathology, progressive loss of motor neurons and muscle dysfunction. Symptom onset can be insidious and diagnosis challenging. Conventional neuroimaging is used to exclude ALS mimics, however more advanced neuroimaging techniques may facilitate an earlier diagnosis. Here, we investigate the potential for neurite orientation dispersion and density imaging and diffusion tensor imaging (DTI) to detect microstructural changes in an experimental model of ALS with neuronal doxycycline (Dox)-suppressible overexpression of human TDP-43 (hTDP-43). *In vivo* diffusion-weighted imaging (DWI) was acquired 1- and 3- weeks following the initiation of hTDP-43 expression (post-Dox) to investigate whether neurite density imaging (NDI) and orientation dispersion imaging (ODI) are affected early in this preclinical model of ALS and if so, how these metrics compare to those derived from the diffusion tensor. Tract-based spatial statistics at 1-week post-Dox, i.e. very early in the disease stage, demonstrated increased NDI in TDP-43 mice but no change in ODI or DTI metrics. At 3-weeks post-Dox, a reduced pattern of increased NDI was observed along with widespread increases in ODI, and decreased fractional anisotropy (FA), apparent diffusion coefficient (ADC) and axial diffusivity (AD). A hypothesis driven analysis of the bilateral corticospinal tracts demonstrated that at 1-week post-Dox, ODI was significantly increased caudally but decreased in the motor cortex of TDP-43 mice. Decreased cortical ODI had normalized by 3-weeks post-Dox and only significant increases were observed. A similar, but inverse pattern in FA was also observed. Together, these results suggest a non-monotonic relationship between DWI metrics and pathophysiological progression with TDP-43 mice exhibiting significantly altered diffusion metrics consistent with early inflammation followed by progressive axonal degeneration. Importantly, significant group-wise changes were observed in the earliest stages of disease when subtle pathology may be more elusive to traditional structural imaging techniques.

1. Introduction

Amyotrophic lateral sclerosis (ALS) is the most common form of motor neuron disease. It is characterized by transactive response DNA-binding protein 43 (TDP-43) pathology and progressive loss of upper and lower motor neurons resulting in muscle dysfunction and then paralysis (Kiernan et al., 2011). Symptom onset is often insidious and with no pathognomonic test for ALS, and a broad spectrum of mimicking disorders, diagnosis remains challenging (Chio, 1999; Palese et al., 2019). A review of 21 retrospective studies published between 1990 and 2020 found a typical diagnostic delay of 10–16 months following symptom presentation with misdiagnosis occurring in 13–68.4% of

Abbreviations: ALS, Amyotrophic lateral sclerosis; CSF, cerebrospinal fluids; Dox, doxycycline; FDC, fibre density and cross-section; FWE, family-wise error; hTDP-43, human TDP-43; NDI, neurite density index; NODDI, neurite orientation dispersion and density imaging; ODI, orientation dispersion index; ROI, region of interest; *NEFH*, neurofilament heavy chain; TBSS, tract-based spatial statistics; TDP-43, transactive response DNA-binding protein 43; ΔNLS, defective nuclear localization signal.

* Corresponding author at: Department of Neuroscience, Central Clinical School, Monash University, The Alfred Centre, 99 Commercial Road, VIC 3004 Australia.
E-mail address: david.wright@monash.edu (D.K. Wright).

https://doi.org/10.1016/j.nicl.2022.103016
Received 10 December 2021; Received in revised form 29 March 2022; Accepted 19 April 2022
Available online 22 April 2022

cases (Richards et al., 2020).

Prompt diagnosis reduces the potential for unnecessary and often invasive procedures, inappropriate or adverse therapeutic avenues, and reduces the associated psychological impact to patients. It also expedites appropriate and supportive interventions, and earlier enrolment into clinical trials of potential disease modifying therapies allowing for both timely initiation of treatment, and extended monitoring of outcomes (Richards et al., 2020). A diagnosis of ALS is made on the widely-accepted El-Escorial revised criteria, which requires both the presence of upper and lower motor neuron degeneration and the progressive spread of symptoms (Brooks et al., 2000). While conventional neuroimaging is currently used to exclude ALS mimics, more advanced neuroimaging techniques may also facilitate a timelier diagnosis (Kiernan et al., 2011).

Diffusion-weighted imaging (DWI) is one neuroimaging technique that may provide sensitive and specific insights into ALS disease progression and in particular, the tissue microstructure. To date, the majority of research investigating DWI in ALS, like other neurodegenerative diseases, has employed diffusion tensor imaging (DTI) (Hobbs et al., 2012; Jack et al., 2015; Kamagata et al., 2021; Kassubek and Muller, 2020; Müller et al., 2016; Wright et al., 2017a; Wright et al., 2017b; Zamani et al., 2021), however its utility as a diagnostic marker is limited, largely stemming from the non-specificity of these metrics to disease pathology (Kamagata et al., 2021; Wright et al., 2017a). DTI determines a single tensor in each voxel and as such, isn't able to distinguish those voxels with a single degenerating fibre bundle (i.e. decreased FA) from those with two or more healthy, but obliquely orientated, fibre bundles (and hence also low FA). Further, as the diffusion tensor models a single tissue type per voxel, DTI metrics are confounded by the presence of extracellular free water in the voxel.

In contrast to DTI, neurite orientation dispersion and density imaging (NODDI) models three different tissue compartments per voxel: intracellular water from within neurites; extra-cellular water from around neurites; and cerebrospinal fluid (Zhang et al., 2012). In doing so, NODDI aims to improve the specificity of DWI by estimating the density of neurites and their dispersion or fanning. A number of studies have investigated NODDI-derived metrics in neurodegenerative disease (Kamiya et al., 2020). In a recent cross-sectional study of ALS, neurite density index (NDI) was found to be significantly reduced in the bilateral corticospinal tracts and transcallosal fibres connecting the primary motor cortices (Broad et al., 2019). These patients also demonstrated reduced neurite orientation dispersion index (ODI) in the precentral gyrus, a finding which correlated with disease duration. Further, when compared to the DTI-derived metric fractional anisotropy (FA), neurite density changes were more widespread, suggesting that in addition to providing greater specificity, NODDI may also be more sensitive in detecting ALS-related white matter pathology (Broad et al., 2019). While promising, additional studies are needed to validate these findings and determine how NODDI metrics change over time (Kamiya et al., 2020).

Employing multimodal MRI, we recently demonstrated progressive neurodegeneration in an experimental model of ALS with neuronal doxycycline (Dox)-suppressible overexpression of human TDP-43 (hTDP-43) (Zamani et al., 2022). These mice underwent *in vivo* MRI at 1- and 3- weeks following the initiation of hTDP-43 expression, including multi-shell DWI which was analyzed using multi-tissue constrained spherical deconvolution. We revisit that data here, employing both DTI and NODDI models to investigate whether neurite density and dispersion are affected in this preclinical model of ALS and if so, how these metrics compare to those derived from the diffusion tensor.

2. Materials and methods

2.1. Study approval

Animal breeding was approved by the University of Queensland Animal Ethics Committee (QBI/040/18). All experimental procedures were approved by the Alfred Research Alliance Animal Ethics Committee (E/1997/2020/M) and conducted in accordance with the Australian Code of Practice for the Care and Use of Animals for Scientific Purposes.

2.2. Subjects

This study included data from 12 adult (10–12 weeks) male mice used in a previous study (Zamani et al., 2022). Of these, 7 were NEFH+/NLS+ (rNLS8) double transgenic mice with Dox-suppressible expression of hTDP-43ΔNLS (referred to as 'TDP-43 mice' throughout) and the remaining 5 NEFH-/NLS + single transgenic littermates were used as controls (Jackson Laboratories NEFH-tTA line 8, stock #025397 and tetO-TARDBP* line 4, stock #014650). The breeding strategy and phenotype of these mice have been described in detail previously (Walker et al., 2015; Wright et al., 2021a). Mice used in the current study were maintained on a pure C57Bl/6JAusb background following ~ 10 generations of backcrossing. Mice were housed in groups under a 12 h/12 h light/dark cycle with *ad libitum* access to food and water. All mice were maintained on a diet containing 200 mg/kg Dox (Diet SF11-059, Specialty Feeds) until the start of the experimental paradigm at which time they were switched to standard chow for the duration of the study.

2.3. DWI acquisition and analysis

At 1- and 3- weeks following the cessation of Dox feed, mice underwent *in vivo* MRI including DWI. Imaging was performed with a 9.4 T Bruker MRI fitted with a BGA12S HP gradient set with a maximum strength of 660 mT/m. Anesthesia was initiated with 4% isoflurane mixed with 100% oxygen and maintained throughout the course of scanning with 1–3% isoflurane. Anaesthetized mice were positioned prone on a cradle with the head fixed in position using ear and bite bars. A hot water system was used to maintain body temperature at 36.5 °C with depth of anesthesia monitored by measuring respiration rate (SA Instruments, Inc). Imaging was performed with actively decoupled surface receive and volume transmit coils.

The shim was optimized using Bruker's MAPSHIM protocol (Kanayama et al., 1996) and a DWI was acquired in the axial plane using a 2D DTI-EPI sequence. Two diffusion shells with b-values of 1500 and 3000 s/mm^2 were acquired in 81 directions. Other parameters included: repetition time = 3600 ms; echo time = 25 ms; number of segments = 1; field of view = 16 × 16 mm^2; matrix size = 64 × 64; 30 slices with thickness = 0.25 mm; δ = 3.5 ms; and Δ = 12 ms. Two b_0 images were also acquired and the total acquisition time was <10 min.

DWI pre-processing and atlas construction was performed as described previously using MRtrix3 (Tournier et al., 2019) and FSL's eddy (Andersson and Sotiropoulos, 2016; Zamani et al., 2022). Pre-processed images were resized to 125 × 125 × 125 μm^3 using cubic interpolation and tensor fitting performed using MRtrix3. The NODDI model was fit to the same pre-processed data using software distributed by the developers (https://www.nitrc.org/projects/noddi_toolbox) and implemented in MATLAB (R2021a, MathWorks, Natick, Massachusetts). DTI and NODDI metrics were registered to atlas space using MRtrix3 and analyzed using tract-based spatial statistics (TBSS) (Smith et al., 2006).

A tract-of-interest analysis was also performed on the bilateral corticospinal tracts. The corticospinal tracts were segmented by identifying tractography streamlines connecting a seed region placed in the motor cortex and a target region in the pons as described previously (Wright et al., 2017b). DTI and NODDI metrics were sampled at 20 equidistant positions along each individual streamline for both left and right tracts (p1, p2, …, p20). The mean of all streamline measurements was then calculated for each position using MATLAB. Measurements were expressed relative to the mean control value at 1 week post-Dox for each corresponding position.

2.4. Statistical analyses

TBSS analyses were performed using the FSL function randomise. Five thousand permutations were run with threshold-free cluster enhancement (Smith and Nichols, 2009) and results were fully corrected for multiple comparisons. Left and right corticospinal tract analyses of diffusion metrics were tested using a general linear model with time as repeated measure (1 and 3 weeks post-Dox) and genotype (TDP-43, control) and position (p1 to p20) as factors. Where multivariate tests for time × genotype × position or time × genotype were significant, post-hoc comparisons were performed with Bonferroni correction. All statistical testing of the corticospinal tracts was performed using IBM SPSS Statistics for Macintosh, Version 27.0 with significance set at $p < 0.05$.

3. Results

3.1. TBSS identified acute increases in intracellular water signal of TDP-43 mice at 1 week post-Dox

One week after the cessation of Dox feed, TBSS analysis demonstrated increased NDI in TDP-43 mice when compared to their littermate controls (Fig. 1). Affected regions included the prelimbic cortex, medial orbital cortex, frontal association cortex, primary and secondary motor cortices, primary somatosensory cortex, forceps minor of the corpus callosum, caudate putamen and external capsule. No significant decreases were observed and there were no significant differences in neurite orientation dispersion or any of the DTI metrics.

3.2. TDP-43 mice exhibit significantly increased intracellular water signal and orientation dispersion at 3 weeks post-Dox

TDP-43 mice also exhibited increased NDI three weeks after the cessation of Dox feed, although not to the extent observed at the earlier 1-week time point (Fig. 2A). In contrast to 1-week post-Dox, TDP-43 mice also demonstrated widespread increases in ODI (Fig. 2B). Affected regions included the fimbria and white matter corresponding to the corticospinal tracts including the internal capsule, cerebral peduncle, substantia nigra and pontine nuclei.

3.3. Altered DTI metrics in TDP-43 mice three weeks after the cessation of Dox feed

TBSS analyses revealed decreased FA (Fig. 3A and D), apparent diffusion coefficient (ADC, Fig. 3B and E) and axial diffusivity (AD, Fig. 3C and F) in TDP-43 mice when compared to littermate controls at 3 weeks post-Dox. Changes in FA were the most widespread of the DTI metrics and included many structures that also exhibited increased ODI – particularly those associated with the corticospinal tracts, the internal capsule, cerebral peduncle, substantia nigra and pontine nuclei. In contrast to the NODDI metrics (Fig. 2B), FA was also reduced in central brain structures corresponding to the thalamic nucleus but was not significantly different in the fimbria.

Brain regions with significantly decreased ADC appeared to correlate with those regions with increased NDI. In particular, the prelimbic cortex, medial orbital cortex, frontal association cortex, and primary and secondary motor cortex ADC values were all significantly different between TDP-43 and littermate control mice. Changes in AD were limited to anterior brain regions including the primary somatosensory cortex, primary motor cortex, and prelimbic cortex.

3.4. TBSS identified longitudinal changes in TDP-43 mice

We compared DTI and NODDI metrics from TDP-43 mice at 1- and 3-weeks post-Dox using TBSS to determine how these metrics changed with disease progression. Compared to 1 week post-Dox, TDP-43 mice had significantly increased ODI (Fig. 4A and B) and decreased FA (Fig. 4C and D) at 3 weeks post-Dox. Significant differences were observed in anterior brain regions corresponding to the primary and secondary motor cortices and the prelimbic cortex. No other significant differences were detected.

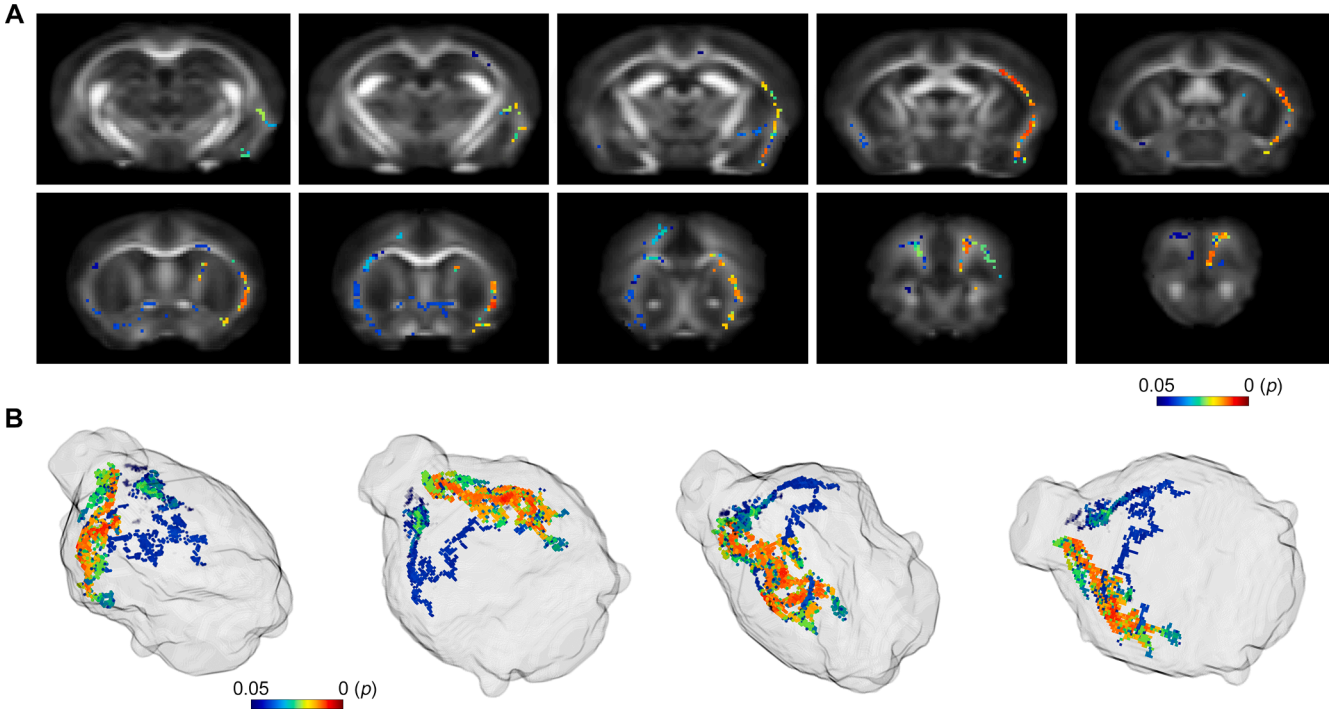

Fig. 1. NODDI revealed early white matter alterations in TDP-43 mice. A) Coronal slices showing significantly increased intra-cellular water signal (NDI) from within the neurites of TDP-43 mice compared to their littermate controls at 1-week post-Dox. Significant voxels are shown overlaid on the study template FA image. B) Obliquely orientated volume renderings of significant voxels shown inside a glass brain. Color bars show FWE-corrected *p*-value.

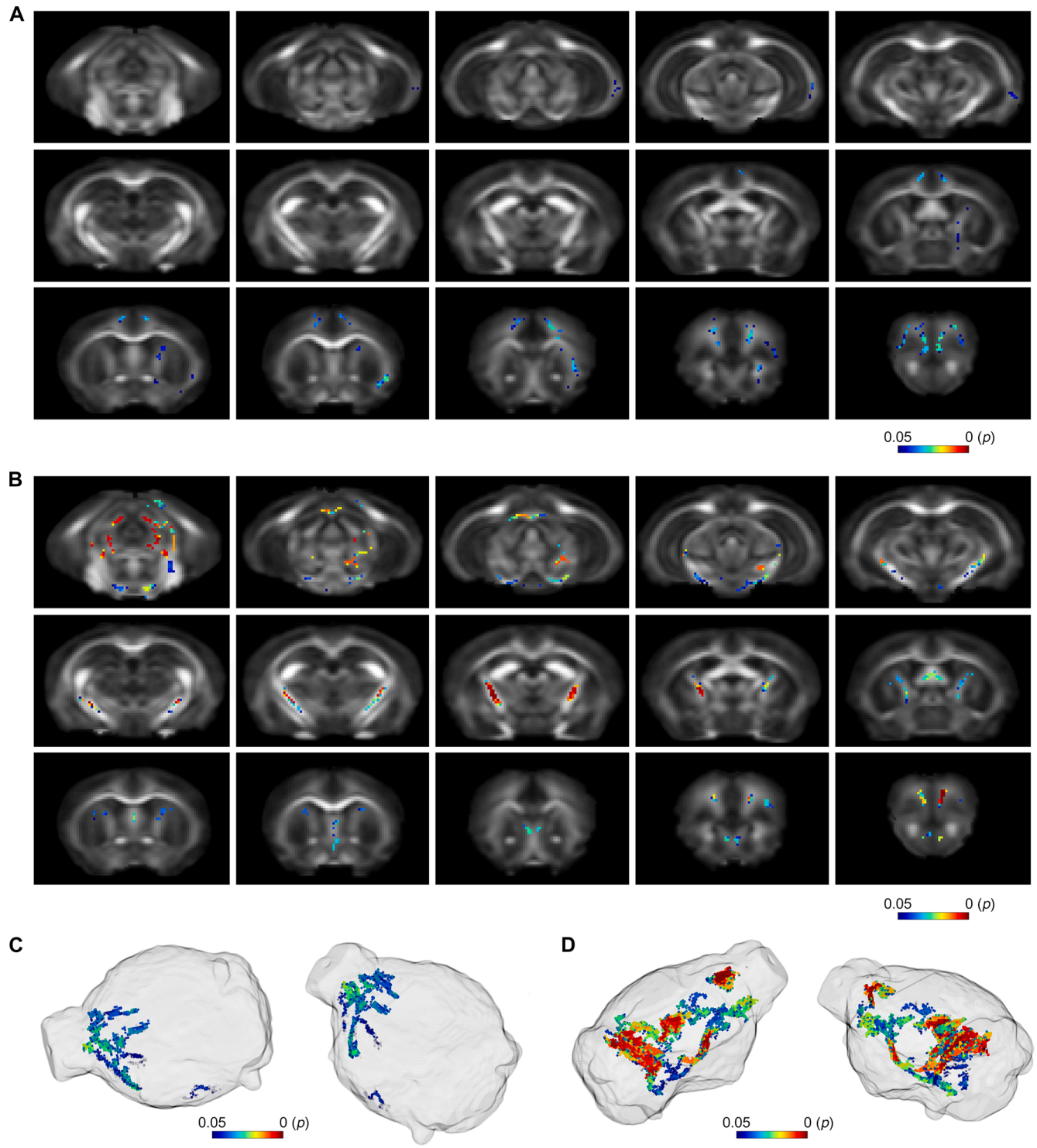

Fig. 2. Three weeks after the cessation of Dox feed, TDP-43 mice exhibited significantly increased white matter neurite density and dispersion. A) TBSS analysis revealed significantly increased NDI in TDP-43 mice when compared to littermate controls. B) TDP-43 mice also exhibited increased neurite orientation dispersion (ODI) 3 weeks after the cessation of Dox feed. Results are shown overlaid on the study template FA image. C) Obliquely orientated volume renderings of significant increased intra-cellular water signal and D) increased neurite orientation dispersion. Color bars show FWE-corrected *p*-value.

3.5. TDP-43 mice exhibit altered diffusion metrics in the corticospinal tracts

In addition to exploratory whole brain analyses, we also performed a hypothesis driven analysis of both NODDI and DTI metrics in the bilateral corticospinal tracts. ALS is defined by progressive degeneration of the corticospinal tracts (Raffelt et al., 2012; Raffelt et al., 2015; Sach et al., 2004; Wright et al., 2017b) and here we found significant differences in a number of diffusion metrics (Fig. 5). In the right hemisphere, there was a significant 3-way interaction for ODI ($F_{19,200}$ = 1.752, p = 0.031, Wilks' Λ = 0.857) with TDP-43 mice having significantly increased ODI 1 week after the cessation of Dox feed at corticospinal tract position p9 ($p < 0.001$) and significantly decreased ODI at positions p19 (p = 0.031) and p20 ($p < 0.001$). At 3 weeks post-Dox,

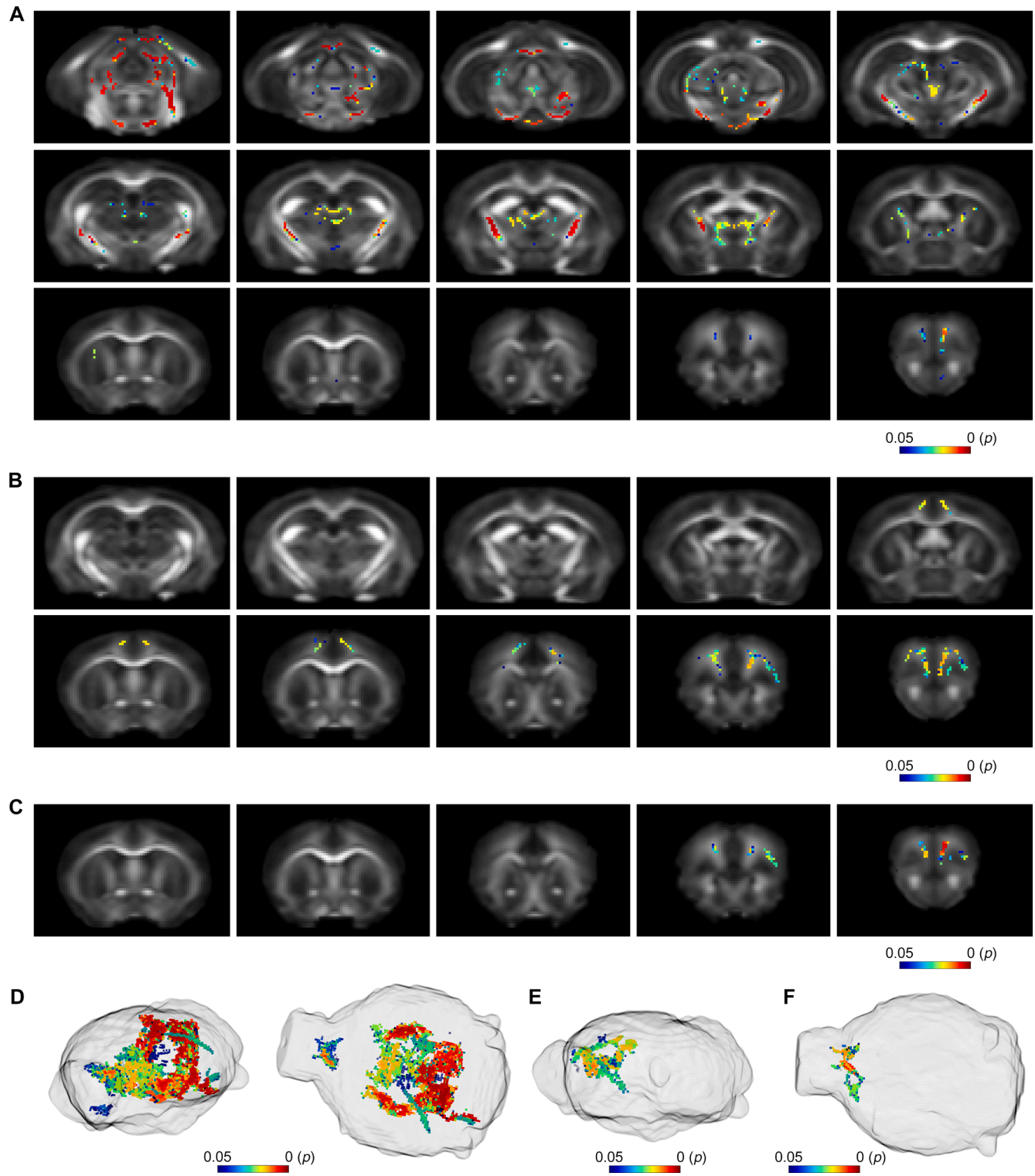

Fig. 3. DTI also reveals microstructural white matter changes in TDP-43 mice three weeks after the cessation of Dox feed. A) TBSS analysis revealed significantly decreased FA in the white matter of TDP-43 mice when compared to their littermate controls. B) TDP-43 mice also demonstrated significantly reduced ADC and C) AD. Significant voxels are shown overlaid on the study template FA image. Obliquely orientated volume renderings of significantly decreased D) FA, E) ADC and F) AD. Color bars show FWE-corrected *p*-value.

significant decreases in ODI were not detected and only significantly increased ODI was observed. Affected corticospinal tract positions included p1 ($p = 0.037$), p8 ($p = 0.004$), p9 ($p = 0.001$), p10 ($p = 0.005$) and p17 ($p = 0.002$). Although not reaching significance, analysis of NDI values revealed a trend ($F_{1,200} = 3.763$, $p = 0.054$, Wilks' $\Lambda = 0.982$) for time × genotype interaction with TDP-43 mice showing increased NDI 1 week after the cessation of Dox feed ($p = 0.007$).

FA also exhibited a significant 3-way interaction ($F_{19,200} = 1.948$, $p = 0.013$, Wilks' $\Lambda = 0.848$) with TDP-43 mice having significantly decreased FA 1 week after the cessation of Dox feed at p8 ($p = 0.049$) and p9 ($p = 0.001$) and significantly increased FA at p18 ($p = 0.005$), p19 ($p = 0.008$) and p20 ($p = 0.006$). At 3 weeks post-Dox, significant

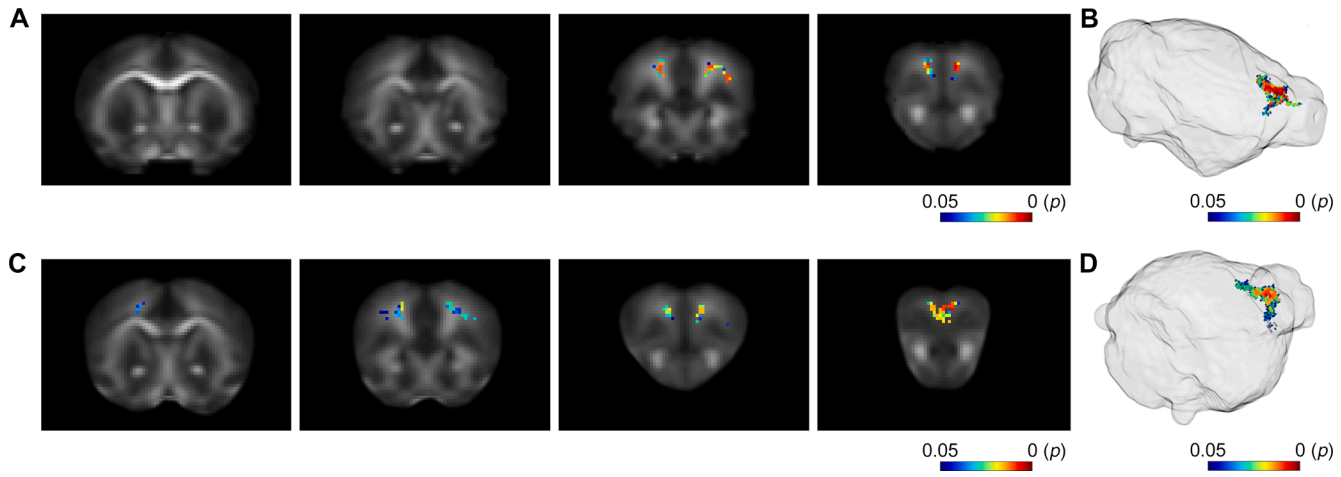

Fig. 4. DWI reveals progressive white matter changes in TDP-43 mice. A) Coronal slices showing TBSS results overlaid on the FA study template image. Increased neurite orientation dispersion (ODI) with B) volume render at right. C) Decreased FA in TDP-43 mice at 3 weeks compared to 1 week post-Dox with D) volume render at right. Color bars show FWE-corrected *p*-value.

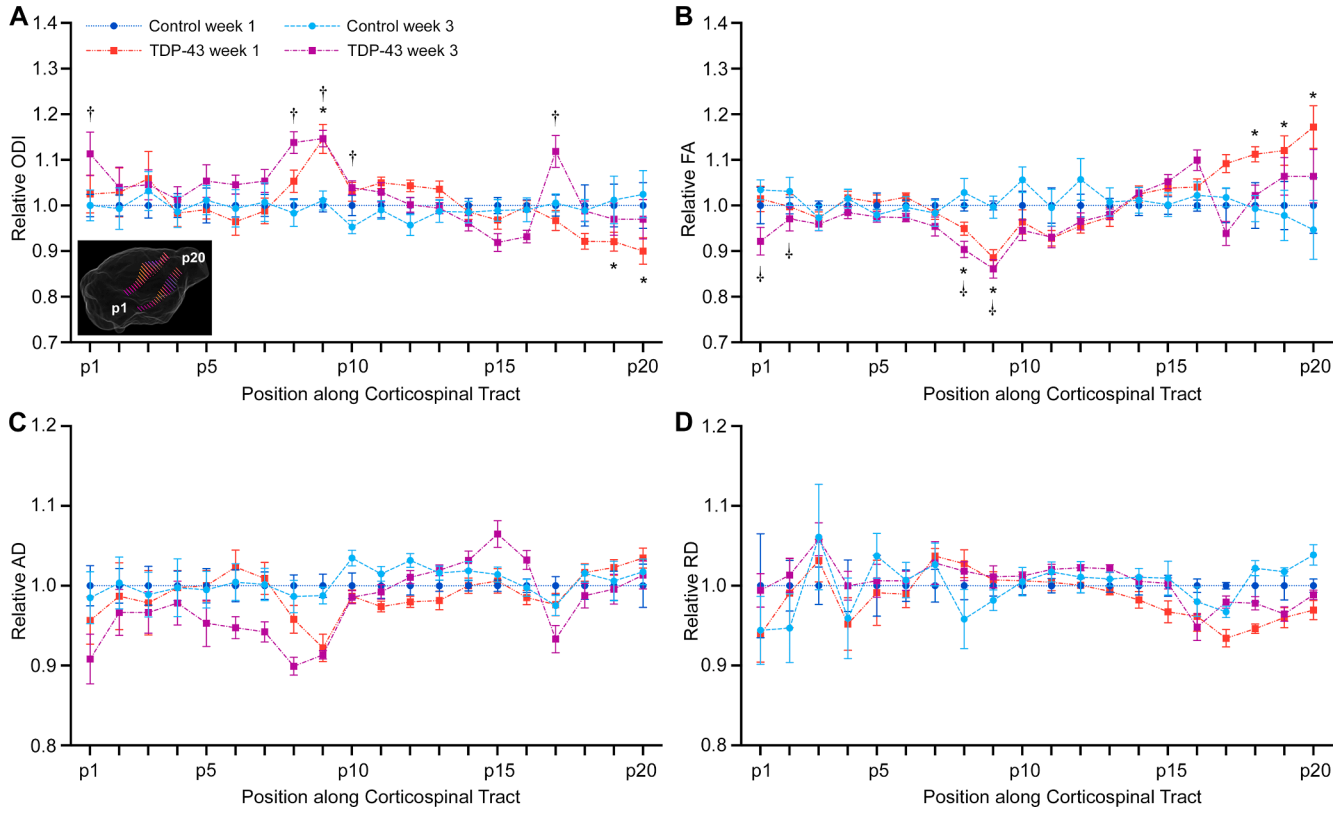

Fig. 5. Altered DWI metrics in the right corticospinal tract of TDP-43 mice. A) Inset shows obliquely orientated glass brain with the segmented and sampled corticospinal tract streamlines. Diffusion metrics were sampled at 20 equidistant positions, from p1 (pons) through to p20 (cortex). Values are expressed relative to the mean value of control mice at the corresponding position at 1-week post-Dox. At 1-week post-Dox, ODI was significantly increased at position p9 but significantly decreased in the motor cortex (positions p19 and p20) of TDP-43 mice. By 3-weeks post-Dox, these cortical decreases had resolved with significantly increased ODI evident at p1, p8-10 and p17. B) Changes in FA were similar but inversed, with significantly decreased FA observed in TDP-43 mice at p8 and p9, and increased FA observed from positions p18-p20. At 3-weeks post-Dox, FA values were significantly reduced at p1, p2, p8 and p9. There were significant interactions between time and genotype for C) AD and D) RD, with TDP-43 mice demonstrating significantly reduced AD at 3-weeks post-Dox and significantly decreased RD at 1-week post-Dox. * Bonferroni corrected $p < 0.05$ at 1-week post-Dox, † Bonferroni corrected $p < 0.05$ at 3 weeks post-Dox. Position of symbol indicates a significant increase (above) or decrease (below) relative to control mice at 1-week post-Dox. Error bars show +/- SEM.

increases in FA were not detected and significantly decreased FA was observed at p1 ($p < 0.001$), p2 ($p = 0.018$), p8 ($p < 0.001$) and p9 ($p = 0.001$). Both AD and radial diffusivity (RD) were significant for time × genotype ($F_{1,200} = 7.643$, $p = 0.006$, Wilks' $\Lambda = 0.963$ and $F_{1,200} = 6.886$, $p = 0.009$, Wilks' $\Lambda = 0.967$, respectively) with TDP-43 mice having significantly decreased AD at 3 weeks ($p < 0.001$) and significantly decreased RD ($p = 0.002$) at 1 week post-Dox.

In the left hemisphere, fewer, but consistent differences were

observed. There were significant interactions between time and genotype for ODI ($F_{1,200} = 4.327$, $p = 0.039$, Wilks' $\Lambda = 0.979$), FA ($F_{1,200} = 8.385$, $p = 0.004$, Wilks' $\Lambda = 0.960$) and AD ($F_{1,200} = 5.210$, $p = 0.024$, Wilks' $\Lambda = 0.975$) with post-hoc comparisons demonstrating significantly decreased AD in TDP-43 mice 3 weeks after the cessation of Dox ($p < 0.001$).

4. Discussion

Despite considerable clinical need, there is currently no recognized diagnostic or prognostic biomarker for ALS. While structural neuroimaging is currently used to exclude ALS mimics, more advanced neuroimaging techniques that interrogate the tissue microstructure may offer greater sensitivity, leading to improved diagnosis and, or, prognosis. However, it has remained unclear how early in disease progression imaging changes may occur in the presence of TDP-43 pathology. We recently demonstrated that the DWI-derived *fixel* metric, fibre density and cross-section, is altered in a transgenic mouse model of ALS that recapitulates TDP-43-related disease. Here, we revisit this data to investigate the potential of NODDI and DTI to also provide insights into ALS disease progression.

There are numerous mouse models of ALS which only variably recapitulate the human disease features (Todd and Petrucelli, 2022). Here, we have chosen the ALS mouse model which best addresses our key questions. The rNLS8 model successfully recapitulates both the characteristic cytoplasmic phosphorylated TDP-43 pathology of ALS in the brain and spinal cord with concurrent brain and muscle atrophy leading to progressive fatal motor decline (Tsitkanou et al., 2022; Walker et al., 2015; Wright et al., 2021a). Diffusion images were acquired at 1- and 3- weeks after the cessation of Dox-feed, which switches on hTDP-43 expression. At 1-week post-Dox, mice have expression of hTDP-43 however cortical thickness, as measured on stained brain sections, remains unaffected (Walker et al., 2015). At around 2-weeks post-Dox, mice show motor impairments, including tremor, and phosphorylated aggregates of hTDP-43, a hallmark of disease pathology. As the time off Dox increases, so too does symptom severity, with cortical atrophy, astrogliosis, muscle neuromuscular junction denervation and worsening motor performance observed before the disease end stage at approximately 10 weeks off Dox (Walker et al., 2015; Wright et al., 2021a). As such, the chosen two imaging timepoints are immediately prior to and after the onset of observable motor phenotypes described previously (Walker et al., 2015; Wright et al., 2021a).

Using TBSS, an exploratory analysis method, we found that only NDI was significantly different between TDP-43 mice and their littermate controls. NDI has been suggested to be more sensitive to white matter pathology than DTI metrics and our results here are consistent with this (Broad et al., 2019; Slattery et al., 2017; Wen et al., 2019). Increased NDI was identified in anterior brain regions including the frontal association cortex, primary motor cortices and somatosensory cortex, the caudate putamen and external capsule. Although NDI is largely reported to be decreased in neurodegenerative disease, including in ALS (Broad et al., 2019; Kamiya et al., 2020), Colgan et al. (2016) reported increased NDI that correlated with hyperphosphorylated tau burden in the cortex and hippocampus of a mouse model of tau pathology (Colgan et al., 2016). More recently, Colon-Perez et al. (2019) also demonstrated increased NDI in the white matter and hippocampus of 8-month-old TgCRND8 mice – a mouse model of Alzheimer's disease with high levels of amyloidosis (Colon-Perez et al., 2019). Interestingly, while decreased NDI has been observed in Alzheimer's disease patients, increased NDI has been observed in cognitively unimpaired individuals with greater amyloid burden but low CSF phosphorylated tau, suggesting a non-monotonic relationship between NDI and pathophysiological progression (Vogt et al., 2021) – i.e. increased NDI in early disease, followed by decreased NDI in later disease stages.

Increased NDI one week after the cessation of Dox may also reflect axonal inflammation and the compression of the extracellular space (Wright et al., 2021c) – a hypothesis supported by our analysis of the corticospinal tracts. We found that while TBSS did not detect any significant differences in ODI or DTI metrics at 1 week post-Dox, tract-of-interest analyses highlighted bi-directional changes in FA and ODI, and decreased RD at this time. Interestingly, increased FA and decreased ODI was observed anteriorly in the motor cortex, while decreased FA and increased ODI were found caudally nearer the pons, potentially highlighting a different underlying pathology in each region. Astrogliosis in response to injury induced inflammation has been associated with increased FA in the grey matter (Budde et al., 2011), while decreased FA is widely considered to be a marker of neurodegeneration (Budde et al., 2011; Wright et al., 2021b; Wright et al., 2017a; Zamani et al., 2021) and a result consistently observed in DTI studies of ALS (Cardenas-Blanco et al., 2016; Chiò et al., 2014; Kassubek and Muller, 2020; Müller et al., 2016; Sach et al., 2004; Smith et al., 2006), including in ALS model mice (Gatto et al., 2019; Müller et al., 2019; Underwood et al., 2011). Hence, one plausible interpretation for the observed changes is that inflammation precedes axonal degeneration and that in these mice, corticospinal tract degeneration occurs in a caudal to rostral direction.

When imaged again at 3-weeks post-Dox, our tract-of-interest analysis demonstrated that elevated FA and decreased ODI in the rostral corticospinal tract had returned to control levels, and only significant increases in ODI and decreases in FA, were detected – consistent with progressive neurodegeneration. At 3 weeks off Dox, TDP-43 mice exhibit greater muscle deficits and worsening ALS phenotype (Walker et al., 2015). Exploratory analyses with TBSS also demonstrated that NDI had largely resolved by this time with significant increases that were largely restricted to anterior brain regions. In contrast, regions of increased ODI and decreased FA were more widespread, including large sections of the corticospinal tracts, consistent with earlier studies in the SOD1^{G93A} mouse model of ALS (Gatto et al., 2019; Gatto et al., 2018).

These findings are also consistent with the results of our initial *fixel*-based analysis of these datasets (Zamani et al., 2022). The term *fixel* refers to an individual fibre bundle within a voxel. In contrast to the diffusion tensor, which describes just a single fibre bundle per voxel, fixel-based analyses can describe, and permit testing of, multiple fibre bundles per voxel. In this earlier work, we undertook connectivity-based fixel enhanced and hypothesis driven analyses of fibre density and cross section (FDC), considered a measure of the overall white matter integrity. Results of these analyses also suggested inflammation at 1 week, i.e. increased FDC, followed by decreased FDC at 3 weeks post-Dox – consistent with neurodegeneration of fibre bundles controlling movement, including primary motor areas and the corticospinal tract.

Here, we also performed direct comparisons of week 1 and week 3 time points with TBSS and found significant increases in ODI and decreases in FA in TDP-43 mice over time. These changes were found anteriorly, in primary and secondary motor cortices and the prelimbic cortex. These findings suggest that despite the widespread neuronal hTDP-43 expression in this mouse model, the motor cortex is uniquely vulnerable. A recent study by Müller and colleagues also reported longitudinal reductions in FA in the primary and secondary motor cortices of TDP-43^{G298S} mice, but in contrast to our results here, not in the corticospinal tract (Müller et al., 2019). This is likely due to the comparatively slower disease progression in TDP-43^{G298S} mice which exhibit very late and asymmetric denervation with no evidence of spinal cord (L4-L5) motor neuron loss even at 2 years of age (Ebstein et al., 2019). In contrast, the mice used here exhibit significant denervation of the tibialis anterior muscle at 4 weeks off Dox and by 8 weeks off Dox have lost approximately half their lumbar spinal cord motor neurons (Walker et al., 2015).

Corticospinal tract degeneration is ubiquitous in ALS and in addition to the observed increase in ODI and decrease in FA, hypothesis driven tract-of-interest analysis also demonstrated significantly decreased AD in TDP-43 mice when compared to littermate controls. Together, these results likely reflect axonal degeneration as demonstrated in a DTI and transmission electron microscopy study of SOD1^{G93A} mouse motor tracts

(Underwood et al., 2011). The longitudinal design of this study precluded a post-mortem analysis and moving forward, additional studies with post-mortem analyses across multiple time points and at later stages of disease are warranted to better understand both the observed non-monotonic relationship between ALS disease progression and diffusion outcomes, as well as the spatial pattern of these changes.

In conclusion, we demonstrate that both NODDI and DTI can detect significant group-wise changes in the rNLS8 TDP-43 mouse model of ALS, including the earliest stages of disease when emerging pathology may be more elusive to traditional structural imaging techniques. Employing both exploratory and hypothesis driven analysis methods, we show that when compared to their littermate controls, TDP-43 mice exhibit significantly altered diffusion metrics consistent with early inflammation in the cortex and progressive axonal degeneration. These results are consistent with an early-stage ALS-like phenotype.

Author contributions

DKW conceptualized and designed the study, performed all analyses, prepared the initial draft of the manuscript and prepared all figures. DKW and AZ collected all data. All authors made substantial contributions to the interpretation of results, critically revised the manuscript and approved the final version.

Declaration of Competing Interest

The authors declare that they have no known competing financial interests or personal relationships that could have appeared to influence the work reported in this paper.

Acknowledgments

This work was supported by the National Health and Medical Research Council to DKW [grant number: 1174040] and AW [fellowship number: 1140386], the Ross Maclean Fellowship and Brazil Family Program for Neurology to AW, and a Bethlehem Griffiths Research Foundation Grant to AZ, AW, and DKW [grant number: BGRF2103]. The authors acknowledge the facilities and scientific and technical assistance of the National Imaging Facility, a National Collaborative Research Infrastructure Strategy (NCRIS) capability at Monash Biomedical Imaging, a Technology Research Platform at Monash University.

References

Andersson, J.L.R., Sotiropoulos, S.N., 2016. An integrated approach to correction for off-resonance effects and subject movement in diffusion MR imaging. Neuroimage 125, 1063–1078.

Broad, R.J., Gabel, M.C., Dowell, N.G., Schwartzman, D.J., Seth, A.K., Zhang, H., Alexander, D.C., Cercignani, M., Leigh, P.N., 2019. Neurite orientation and dispersion density imaging (NODDI) detects cortical and corticospinal tract degeneration in ALS. J. Neurol. Neurosurg. Psychiatry 90, 404–411.

Brooks, B.R., Miller, R.G., Swash, M., Munsat, T.L., World Federation of Neurology Research Group on Motor Neuron, D, 2000. El Escorial revisited: revised criteria for the diagnosis of amyotrophic lateral sclerosis. Amyotroph. Lateral Scler. Other Motor Neuron Disord. 1, 293–299.

Budde, M.D., Janes, L., Gold, E., Turtzo, L.C., Frank, J.A., 2011. The contribution of gliosis to diffusion tensor anisotropy and tractography following traumatic brain injury: validation in the rat using Fourier analysis of stained tissue sections. Brain 134, 2248–2260.

Cardenas-Blanco, A., Machts, J., Acosta-Cabronero, J., Kaufmann, J., Abdulla, S., Kollewe, K., Petri, S., Schreiber, S., Heinze, H.J., Dengler, R., Vielhaber, S., Nestor, P. J., 2016. Structural and diffusion imaging versus clinical assessment to monitor amyotrophic lateral sclerosis. Neuroimage Clin 11, 408–414.

Chio, A., 1999. ISIS Survey: an international study on the diagnostic process and its implications in amyotrophic lateral sclerosis. J. Neurol. 246 (Suppl 3), III1-5.

Chiò, A., Pagani, M., Agosta, F., Calvo, A., Cistaro, A., Filippi, M., 2014. Neuroimaging in amyotrophic lateral sclerosis: insights into structural and functional changes. Lancet Neurol. 13, 1228–1240.

Colgan, N., Siow, B., O'Callaghan, J.M., Harrison, I.F., Wells, J.A., Holmes, H.E., Isail, O., Richardson, S., Alexander, D.C., Collins, E.C., Fisher, E.M., Johnson, R., Schwarz, A. J., Ahmed, Z., O'Neill, M.J., Murray, T.K., Zhang, H., Lythgoe, M.F., 2016. Application of neurite orientation dispersion and density imaging (NODDI) to a tau pathology model of Alzheimer's disease. Neuroimage 125, 739–744.

Colon-Perez, L.M., Ibanez, K.R., Suarez, M., Torroella, K., Acuna, K., Ofori, E., Levites, Y., Vaillancourt, D.E., Golde, T.E., Chakrabarty, P., Febo, M., 2019. Neurite orientation dispersion and density imaging reveals white matter and hippocampal microstructure changes produced by Interleukin-6 in the TgCRND8 mouse model of amyloidosis. Neuroimage 202, 116138.

Ebstein, S.Y., Yagudayeva, I., Shneider, N.A., 2019. Mutant TDP-43 causes early-stage dose-dependent motor neuron degeneration in a TARDBP knockin mouse model of ALS. Cell Rep. 26 (364–373), e364.

Gatto, R.G., Mustafi, S.M., Amin, M.Y., Mareci, T.H., Wu, Y.C., Magin, R.L., 2018. Neurite orientation dispersion and density imaging can detect presymptomatic axonal degeneration in the spinal cord of ALS mice. Funct. Neurol. 33, 155–163.

Gatto, R.G., Amin, M., Finkielsztein, A., Weissmann, C., Barrett, T., Lamoutte, C., Uchitel, O., Sumagin, R., Mareci, T.H., Magin, R.L., 2019. Unveiling early cortical and subcortical neuronal degeneration in ALS mice by ultra-high field diffusion MRI. Amyotroph. Lateral Scler. Frontotemporal Degener. 20, 549–561.

Hobbs, N.Z., Cole, J.H., Farmer, R.E., Rees, E.M., Crawford, H.E., Malone, I.B., Roos, R. A., Sprengelmeyer, R., Durr, A., Landwehrmeyer, B., Scahill, R.I., Tabrizi, S.J., Frost, C., 2012. Evaluation of multi-modal, multi-site neuroimaging measures in Huntington's disease: baseline results from the PADDINGTON study. Neuroimage Clin. 2, 204–211.

Jack Jr., C.R., Barnes, J., Bernstein, M.A., Borowski, B.J., Brewer, J., Clegg, S., Dale, A. M., Carmichael, O., Ching, C., DeCarli, C., Desikan, R.S., Fennema-Notestine, C., Fjell, A.M., Fletcher, E., Fox, N.C., Gunter, J., Gutman, B.A., Holland, D., Hua, X., Insel, P., Kantarci, K., Killiany, R.J., Krueger, G., Leung, K.K., Mackin, S., Aillard, P., Malone, I.B., Mattsson, N., McEvoy, L., Modat, M., Mueller, S., Nosheny, R., Ourselin, S., Schuff, N., Senjem, M.L., Simonson, A., Thompson, P.M., Rettmann, D., Vemuri, P., Walhovd, K., Zhao, Y., Zuk, S., Weiner, M., 2015. Magnetic resonance imaging in Alzheimer's Disease Neuroimaging Initiative 2. Alzheimers Dement. 11, 740–756.

Kamagata, K., Andica, C., Kato, A., Saito, Y., Uchida, W., Hatano, T., Lukies, M., Ogawa, T., Takeshige-Amano, H., Akashi, T., Hagiwara, A., Fujita, S., Aoki, S., 2021. Diffusion magnetic resonance imaging-based biomarkers for neurodegenerative diseases. Int. J. Mol. Sci. 22.

Kamiya, K., Hori, M., Aoki, S., 2020. NODDI in clinical research. J. Neurosci. Methods 346, 108908.

Kanayama, S., Kuhara, S., Satoh, K., 1996. In vivo rapid magnetic field measurement and shimming using single scan differential phase mapping. Magn. Reson. Med. 36, 637–642.

Kassubek, J., Muller, H.P., 2020. Advanced neuroimaging approaches in amyotrophic lateral sclerosis: refining the clinical diagnosis. Expert Rev. Neurother. 20, 237–249.

Kiernan, M.C., Vucic, S., Cheah, B.C., Turner, M.R., Eisen, A., Hardiman, O., Burrell, J.R., Zoing, M.C., 2011. Amyotrophic lateral sclerosis. Lancet 377, 942–955.

Müller, H.P., Turner, M.R., Grosskreutz, J., Abrahams, S., Bede, P., Govind, V., Prudlo, J., Ludolph, A.C., Filippi, M., Kassubek, J., Neuroimaging Society in, A.L.S.D.T.I.S.G, 2016. A large-scale multicentre cerebral diffusion tensor imaging study in amyotrophic lateral sclerosis. J. Neurol. Neurosurg. Psychiatry 87, 570–579.

Müller, H.P., Brenner, D., Roselli, F., Wiesner, D., Abaei, A., Gorges, M., Danzer, K.M., Ludolph, A.C., Tsao, W., Wong, P.C., Rasche, V., Weishaupt, J.H., Kassubek, J., 2019. Longitudinal diffusion tensor magnetic resonance imaging analysis at the cohort level reveals disturbed cortical and callosal microstructure with spared corticospinal tract in the TDP-43 (G298S) ALS mouse model. Transl. Neurodegener. 8, 27.

Palese, F., Sartori, A., Logroscino, G., Pisa, F.E., 2019. Predictors of diagnostic delay in amyotrophic lateral sclerosis: a cohort study based on administrative and electronic medical records data. Amyotroph. Lateral Scler. Frontotemporal Degener. 20, 176–185.

Raffelt, D.A., Smith, R.E., Ridgway, G.R., Tournier, J.D., Vaughan, D.N., Rose, S., Henderson, R., Connelly, A., 2015. Connectivity-based fixel enhancement: whole-brain statistical analysis of diffusion MRI measures in the presence of crossing fibres. Neuroimage 117, 40–55.

Raffelt, D., Tournier, J.D., Rose, S., Ridgway, G.R., Henderson, R., Crozier, S., Salvado, O., Connelly, A., 2012. Apparent Fibre Density: a novel measure for the analysis of diffusion-weighted magnetic resonance images. Neuroimage 59, 3976–3994.

Richards, D., Morren, J.A., Pioro, E.P., 2020. Time to diagnosis and factors affecting diagnostic delay in amyotrophic lateral sclerosis. J. Neurol. Sci. 417, 117054.

Sach, M., Winkler, G., Glauche, V., Liepert, J., Heimbach, B., Koch, M.A., Buchel, C., Weiller, C., 2004. Diffusion tensor MRI of early upper motor neuron involvement in amyotrophic lateral sclerosis. Brain 127, 340–350.

Slattery, C.F., Zhang, J., Paterson, R.W., Foulkes, A.J.M., Carton, A., Macpherson, K., Mancini, L., Thomas, D.L., Modat, M., Toussaint, N., Cash, D.M., Thornton, J.S., Henley, S.M.D., Crutch, S.J., Alexander, D.C., Ourselin, S., Fox, N.C., Zhang, H., Schott, J.M., 2017. ApoE influences regional white-matter axonal density loss in Alzheimer's disease. Neurobiol. Aging 57, 8–17.

Smith, S.M., Nichols, T.E., 2009. Threshold-free cluster enhancement: addressing problems of smoothing, threshold dependence and localisation in cluster inference. Neuroimage 44, 83–98.

Smith, S.M., Jenkinson, M., Johansen-Berg, H., Rueckert, D., Nichols, T.E., Mackay, C.E., Watkins, K.E., Ciccarelli, O., Cader, M.Z., Matthews, P.M., Behrens, T.E., 2006. Tract-based spatial statistics: voxelwise analysis of multi-subject diffusion data. Neuroimage 31, 1487–1505.

Todd, T.W., Petrucelli, L., 2022. Modelling amyotrophic lateral sclerosis in rodents. Nat. Rev. Neurosci. 23, 231–251.

Tournier, J.D., Smith, R., Raffelt, D., Tabbara, R., Dhollander, T., Pietsch, M., Christiaens, D., Jeurissen, B., Yeh, C.H., Connelly, A., 2019. MRtrix3: A fast, flexible

and open software framework for medical image processing and visualisation. Neuroimage 202, 116137.
Tsitkanou, S., Della Gatta, P.A., Abbott, G., Wallace, M.A., Lindsay, A., Gerlinger-Romero, F., Walker, A.K., Foletta, V.C., Russell, A.P., 2022. miR-23a suppression accelerates functional decline in the rNLS8 mouse model of TDP-43 proteinopathy. Neurobiol. Dis. 162, 105559.
Underwood, C.K., Kurniawan, N.D., Butler, T.J., Cowin, G.J., Wallace, R.H., 2011. Non-invasive diffusion tensor imaging detects white matter degeneration in the spinal cord of a mouse model of amyotrophic lateral sclerosis. Neuroimage 55, 455–461.
Vogt, N.M., Hunt, J.F.V., Adluru, N., Ma, Y., Van Hulle, C.A., Iii, D.C.D., Kecskemeti, S.R., Chin, N.A., Carlsson, C.M., Asthana, S., Johnson, S.C., Kollmorgen, G., Batrla, R., Wild, N., Buck, K., Zetterberg, H., Alexander, A.L., Blennow, K., Bendlin, B.B., 2021. Interaction of amyloid and tau on cortical microstructure in cognitively unimpaired adults. Alzheimers Dement.
Walker, A.K., Spiller, K.J., Ge, G., Zheng, A., Xu, Y., Zhou, M., Tripathy, K., Kwong, L.K., Trojanowski, J.Q., Lee, V.M., 2015. Functional recovery in new mouse models of ALS/FTLD after clearance of pathological cytoplasmic TDP-43. Acta Neuropathol. 130, 643–660.
Wen, J., Zhang, H., Alexander, D.C., Durrleman, S., Routier, A., Rinaldi, D., Houot, M., Couratier, P., Hannequin, D., Pasquier, F., Zhang, J., Colliot, O., Le Ber, I., Bertrand, A., Predict to Prevent Frontotemporal Lobar, D., Amyotrophic Lateral Sclerosis Study, G, 2019. Neurite density is reduced in the presymptomatic phase of C9orf72 disease. J. Neurol. Neurosurg. Psychiatry 90, 387–394.
Wright, A.L., Della Gatta, P.A., Le, S., Berning, B.A., Mehta, P., Jacobs, K.R., Gul, H., San Gil, R., Hedl, T.J., Riddell, W.R., Watson, O., Keating, S.S., Venturato, J., Chung, R. S., Atkin, J.D., Lee, A., Shi, B., Blizzard, C.A., Morsch, M., Walker, A.K., 2021a. Riluzole does not ameliorate disease caused by cytoplasmic TDP-43 in a mouse model of amyotrophic lateral sclerosis. Eur. J. Neurosci. 54, 6237–6255.
Wright, D.K., Johnston, L.A., Kershaw, J., Ordidge, R., O'Brien, T.J., Shultz, S.R., 2017a. Changes in apparent fiber density and track-weighted imaging metrics in white matter following experimental traumatic brain injury. J. Neurotrauma 34, 2109–2118.
Wright, D.K., Liu, S., van der Poel, C., McDonald, S.J., Brady, R.D., Taylor, L., Yang, L., Gardner, A.J., Ordidge, R., O'Brien, T.J., Johnston, L.A., Shultz, S.R., 2017b. Traumatic brain injury results in cellular, structural and functional changes resembling motor neuron disease. Cereb. Cortex 27, 4503–4515.
Wright, D.K., Gardner, A.J., Wojtowicz, M., Iverson, G.L., O'Brien, T.J., Shultz, S.R., Stanwell, P., 2021b. White matter abnormalities in retired professional rugby league players with a history of concussion. J. Neurotrauma 38, 983–988.
Wright, D.K., Symons, G.F., O'Brien, W.T., McDonald, S.J., Zamani, A., Major, B., Chen, Z., Costello, D., Brady, R.D., Sun, M., Law, M., O'Brien, T.J., Mychasiuk, R., Shultz, S.R., 2021c. Diffusion imaging reveals sex differences in the white matter following sports-related concussion. Cereb. Cortex 31, 4411–4419.
Zamani, A., O'Brien, T.J., Kershaw, J., Johnston, L.A., Semple, B.D., Wright, D.K., 2021. White matter changes following experimental pediatric traumatic brain injury: an advanced diffusion-weighted imaging investigation. Brain Imaging Behav. 15, 2766–2774.
Zamani, A., Walker, A.K., Rollo, B., Ayers, K.L., Farah, R., O'Brien, T.J., Wright, D.K., 2022. Impaired glymphatic function in the early stages of disease in a TDP-43 mouse model of amyotrophic lateral sclerosis. Transl. Neurodegener. 11, 17.
Zhang, H., Schneider, T., Wheeler-Kingshott, C.A., Alexander, D.C., 2012. NODDI: practical in vivo neurite orientation dispersion and density imaging of the human brain. Neuroimage 61, 1000–1016.